Applied Catalysis B: Environmental 239 (2018) 578–585

Contents lists available at ScienceDirect

Applied Catalysis B: Environmental

journal homepage: www.elsevier.com/locate/apcatb

Robust photocatalytic hydrogen evolution over amorphous ruthenium phosphide quantum dots modified g-C_3N_4 nanosheet

Junfang Wang[1], Juan Chen[1], Peifang Wang, Jun Hou, Chao Wang, Yanhui Ao*

Key Laboratory of Integrated Regulation and Resource Development on Shallow Lakes, Ministry of Education, College of Environment, Hohai University, No.1, Xikang road, Nanjing, 210098, China

ARTICLE INFO

Keywords:
Amorphous ruthenium phosphide
g-C_3N_4
Cocatalysts
Hydrogen evolution performance

ABSTRACT

The development of materials which meet the needs of both cost-efficiency and high performance for hydrogen evolution reaction is of great importance. However, developing photocatalysts with Pt-like activity still remains as a major challenge. Herein, we utilize ultrafine amorphous ruthenium phosphide (RP) nanoparticles as a high-efficient and robust cocatalyst to enhance the H_2 production activity of g-C_3N_4 (g-CN). The RP/g-CN samples were prepared based on a facile in-situ growth phosphatization method. The optimum H_2 evolution rate reached up to 2110 μmol $h^{-1}g^{-1}$ for 0.1%-RP/g-CN, which was 113.4 times as high as that of pristine g-C_3N_4 and 2.22 times of Pt-loaded g-C_3N_4. Furthermore, ruthenium is the cheapest platinum-group metal and its amount in the best RP/g-CN sample is only 0.1%, showing the superiority of competitive price and high activity. The introduction of ultrafine amorphous ruthenium phosphide accelerated the transfer rate of electrons and restrain the recombination of charge carriers. The amorphous ruthenium phosphide ultrafine nanoparticles could also serve as cocatalysts for hydrogen evolution. This work provides a promising alternative to expensive Pt-loaded photocatalyst for excellent hydrogen evolution performance under visible light irradiation.

1. Introduction

There is an urgency to explore a clean, renewable and sustainable energy resource to suppress the environmental problems associated with CO_2 emission from fossil fuels [1–5]. Among the alternative energy sources, hydrogen energy is an ideal promising option to achieve the pollution abatement and environmental remediation [6–9]. Thus photocatalytic water splitting, using simulated solar light, has been an attractive route and evokes increasing attention. Until now, various semiconductor photocatalysts including oxides [10–12], sulfides [13–15], nitrides [16–18], carbides [19,20], etc, have been developed. Unfortunately, the majority of them are limited by their wide band gap, high-cost or low stability and none of them can be used in the practical application [21].

Recently, a 2D polymer-like metal-free photocatalyst, graphitic carbon nitride (g-C_3N_4) has enthralled increasing interest owing to its suitable band gap (2.7 eV), specific planer structure, great stability, low-cost and abundance in raw materials on the earth [22–26]. However, the weak absorption of the visible light and fast recombination of photogenerated charge carriers seriously limit the photocatalytic performance of pure g-C_3N_4 [27,28].

For decades, enormous efforts have been paid to enhance the hydrogen yield, including porosity engineering [29,30], doping foreign metal or non-metal elements [31,32], creating heterojunction [12,33]. Among them, combining with a cocatalyst has been regarded as a facile and effective approach to overcome the aforementioned issues [34,35]. Recently, metal phosphides, including Ni_2P [36,37], CoP [38,39], MoP [40], and FeP [8], have been thrust into the limelight as excellent cocatalysts for photocatalytic H_2 evolution with the similar properties as zero-valent metals [41]. For instance, Zhao et al. prepared the Ni_2P/g-C_3N_4 hybrid photocatalyst that showed great hydrogen production performance which resulted from the fast separation and transfer rate of photogenerated electrons and low charge carriers recombination [42]. Yan et al. reported the remarkable H_2 evolution efficiency of CoP/g-C_3N_4 in the presence of CoP cocatalyst [24].

Nevertheless, their performance remained largely subpar as compared to Pt-based g-C_3N_4 [43]. It is of great significance to explore applicable alternatives due to the scarcity and valuableness of Pt (992 $ per oz). To date, the use of other lower-cost platinum-group metals, such as palladium (551 $ per oz), iridium (500 $ per oz) [44–46], and ruthenium (42 $ per oz) is increasing. In particular, Ru-based photocatalysts has been proved to be a robust and efficient alternative

* Corresponding author.
E-mail address: andyao@hhu.edu.cn (Y. Ao).
[1] This two authors contribute equally to the work.

https://doi.org/10.1016/j.apcatb.2018.08.048
Received 1 May 2018; Received in revised form 5 August 2018; Accepted 18 August 2018
Available online 19 August 2018

catalysts for hydrogen evolution reaction [47–49]. According to the previous report of Ru_2P/RGO material, ultrasmall Ru_2P nanoparticles grown on RGO showed extremely high hydrogen evolution performance [50]. However, to the best of our knowledge, there is few relevant research available in the literature about ruthenium phosphide as cocatalyst supported on the surface of g- C_3N_4 to improve photocatalytic hydrogen generation.

Inspired by the effect of phosphatization and the character of ruthenium, in this work, we introduced ultrafine amorphous ruthenium phosphide nanoparticles into g-C_3N_4, via a facile in-situ phosphatization method. The obtained RP/g-CN hybrid materials showed an unprecedented high photocatalytic performance towards hydrogen evolution, even superior to Pt-based g-C_3N_4.

2. Experimental section

2.1. Materials

Urea, ruthenium chloride hydrate ($RuCl_3{\cdot}3H_2O$), sodium hypophosphite ($NaH_2PO_2{\cdot}H_2O$) and ethanol. All chemicals in this work were of analytical grade, obtained from Sinopharm Chemical Reagent Co., Ltd, and used without additional purification.

2.2. Preparation of photocatalysts

2.2.1. Preparation of g-C_3N_4

The g-C_3N_4 was synthesized following the typical thermal treatment of urea as reported previously [51,52]. 10 g of urea was added into a covered crucible and heated at 600℃ for 2 h in a muffle furnace at a heating rate of 5 ℃/min. The resultant light yellow-colored product was ultrasonicated with distill water for 10 min and then filtered and dried at 60℃ for more than 10 h to obtain g-C_3N_4 (denoted as g-CN).

2.2.2. Preparation of Ru-g-CN

200 mg of as-prepared g-CN was dispersed into 100 mL distill water and then ultrasonicated for 1 h to form uniform aqueous suspension. After that, the resultant suspension was transferred into an oil bath and heated at 70 ℃. 2 mg/mL $RuCl_3{\cdot}3H_2O$ was added into g-CN homogeneous solution with different ruthenium mass ratio (0.05%, 0.1%, 0.2%, 0.5%, 1% of the g-CN). Then the mixture was kept at 70℃ for reflux with continuous stirring for 24 h. The rotary evaporation procedure was then applied to dry the as-obtained mixture. The obtained grey solid was then grounded into fine powder. Finally, the Ru-oxo/g-C_3N_4 (denoted as Ru-g-CN) was synthesized by annealing the powder at 400℃in a crucible.

2.2.3. Preparation of amorphous ruthenium phosphide modified g-CN

50 mg of as-prepared Ru-g-CN sample and 50 mg of sodium hypophosphite (NaH_2PO_2) were mixed uniformly and then annealed at 300 ℃ for 2 h at a ramp rate of 2 ℃min^{-1} in argon atmosphere. The powder obtained (denoted as RP/g-CN) was then washed with pure water and ethanol for 4 times and dried in an oven for more than 10 h.

2.3. Characterization of samples

Powder X-ray diffraction (XRD) was measured to analysis the structure of samples with a Rigaku / Smartlab diffractometer under Cu Kα radiation (λ = 0.15418 nm) at 40 Kv and 40 mA. Transmission electron microscopy (TEM) images were recorded by JEM-2100 (JEOL, Japan). X-ray photoelectron spectroscopy (XPS) was employed to estimate the binding energies and chemical composion of elements. The XPS was done on a Thermo Scientific ESCALAB 250 instrument with Al Kα source. The Shimadzu UV-3600 ultraviolet-visible spectrometer was used to test the optical properties of as-prepared samples. Photoluminescence (PL) spectra was collected on a Hitachi F-700 fluorescence Spectrophotometer with an excitation wavelength of 200 nm at room temperature. Time-resolved PL spectra were carried out on a FLS980 spectrofluorometer (Edinburgh Instruments) with excitation wavelength of 330 nm.

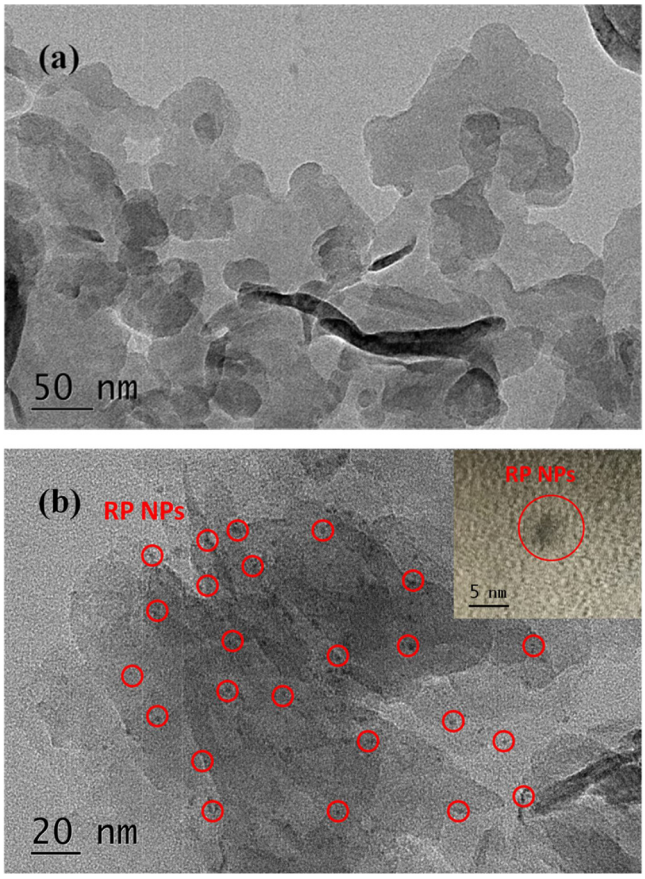

Fig. 1. The TEM images of (a) as-prepared pure g-CN, (b) 0.1%-RP/g-CN and HRTEM image of 0.1%-RP/g-CN (insert).

2.4. Activity tests

The photocatalytic water-splitting of the obtained samples was carried out in a gas-closed system. Typically, 10 mg of photocatalyst powder was added into 50 ml of aqueous solution containing 10 vol % triethanolamine (TEOA) which served as the sacrificial agent. In order to achieve a uniformly dispersion, the system was ultrasonicated for about 10 min. The suspension was evacuated with the assistance of a vacuum pump for 30 min to ensure the anaerobic condition. The well dispersed solution was then irradiated by a 300 W Xe lamp coupled with a cut-off filter (420 nm) under continuous stirring. The hydrogen evolution was quantified by an online gas chromatograph using N_2 as the carrier gas (GC-7900. TCD) every 1 h and lasted for 4 h.

2.5. Photoelectrochemical measurements

The photoelectrochemical properties was performed on an electrochemical analyzer (CHI660D, Chenhua Instrument, Shanghai, China). The corresponding catalyst film coated FTO, Pt plate and Ag/AgCl served as working electrode, counter electrode and reference electrode, respectively. The working electrode was fabricated according to the method reported previously [53]: 5 mg of sample was dispersed in 980 μL water/ethanol (v/v = 1:1) mixture along with 20 μL 5 wt% of Nafion solution and then was ultrasonic treated for 30 min to form homogeneous slurry. Then, the suspension was uniformly dropped on a 1 × 1 cm^2 FTO glass. The photocurrent response of samples was measured in 0.5 M Na_2SO_4 aqueous solution under visible light provided by

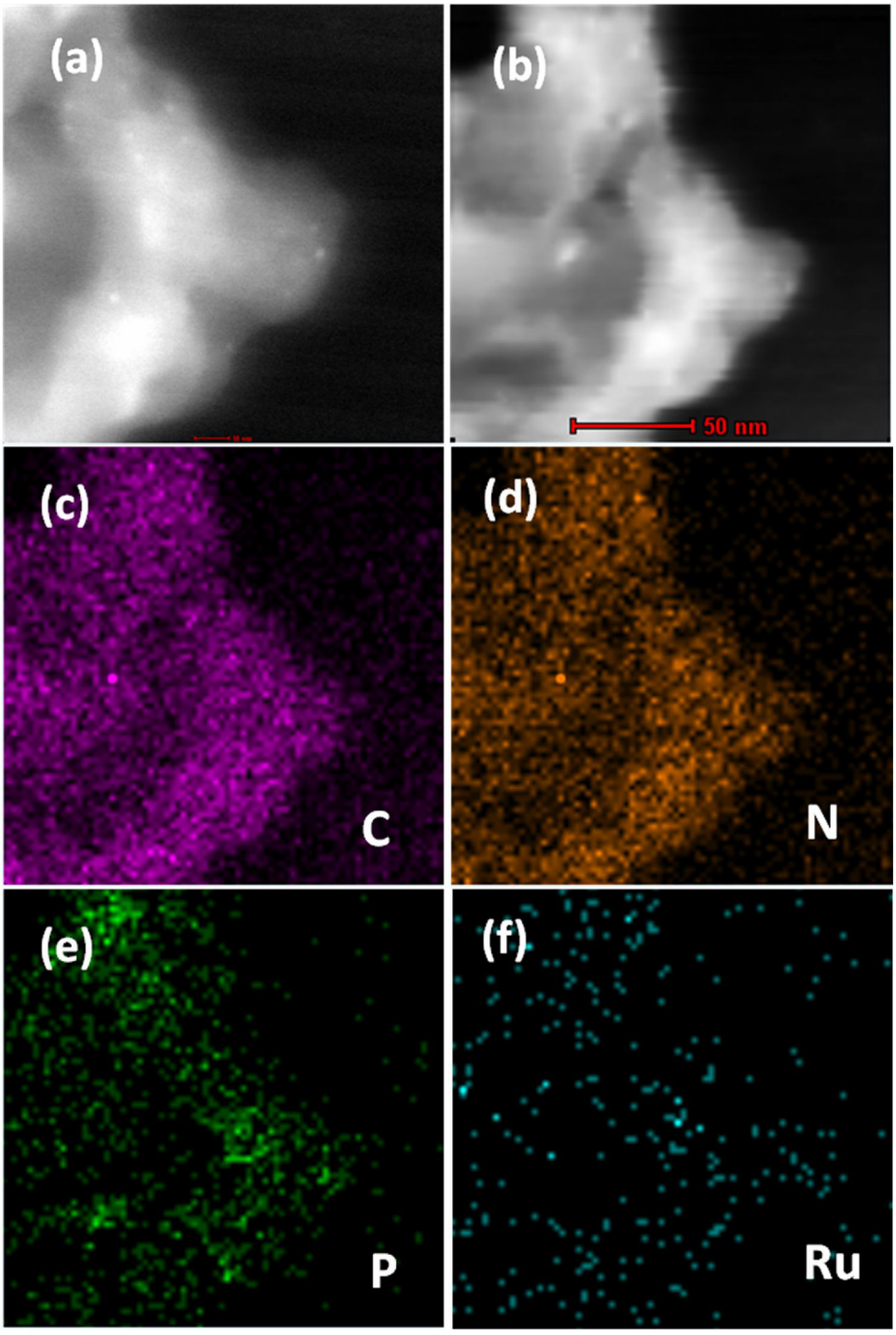

Fig. 2. (a) STEM (scale bar 10 nm) and (b–f) elemental mapping images of 0.1%-RP/g-CN.

a 300 W xenon arc lamp. The Electrochemical impedance spectroscopy (EIS) was obtained in 0.5 M Na_2SO_4 aqueous solution at a bias voltage of 0.3 V over the frequency range from 10^5 to 0.01 Hz. The linear sweep voltammetry (LSV) was conducted in 0.5 M H_2SO_4 electrolyte solution. Glassy carbon electrode, carbon rod and Ag/AgCl were used as working, counter and reference electrode, respectively.

3. Results and discussion

3.1. Physicochemical property

To reveal the morphology and microstructure of prepared samples, the TEM images of pristine g-CN and 0.1%-RP/g-CN were collected. As shown in Fig. 1, both g-CN and 0.1%-RP/g-CN displayed the typical 2D nanosheet morphology. However, it was clear that there were a large amount of ultrafine black dots well dispersed on the surface of C_3N_4 in sample 0.1%-RP/g-CN with no aggregation. Unfortunately, no lattice fringes of ruthenium phosphide could be seen in Fig. 1b insert, indicating the amorphous nature of the ultrafine ruthenium phosphide nanoparticles (RP NPs) in the RP/g-CN composites.

According to the STEM image (10 nm) of 0.1%-RP/g-CN (Fig. 2a), it can be seen that many white nanoparticles (approximately 2 nm) dispersed uniformly on the g-CN surface. Furthermore, the STEM elemental mapping of 0.1%-RP/g-CN (Fig. 2b-f) confirmed the presence of

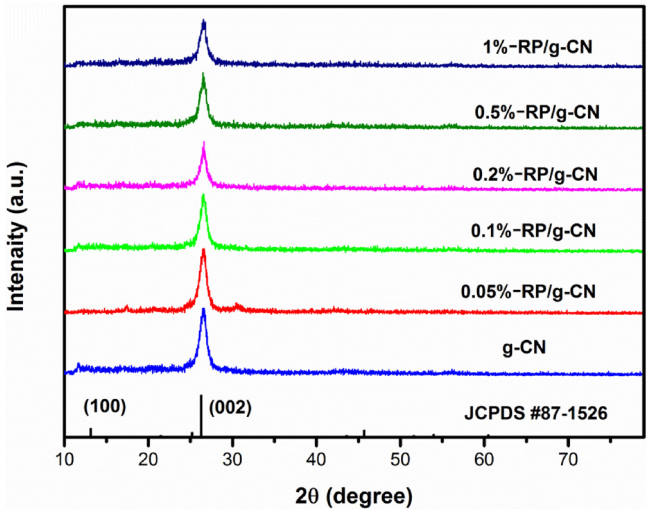

Fig. 3. The XRD patterns of pristine g-CN and as-prepared RP/g-CN composites with different ruthenium phosphide contents.

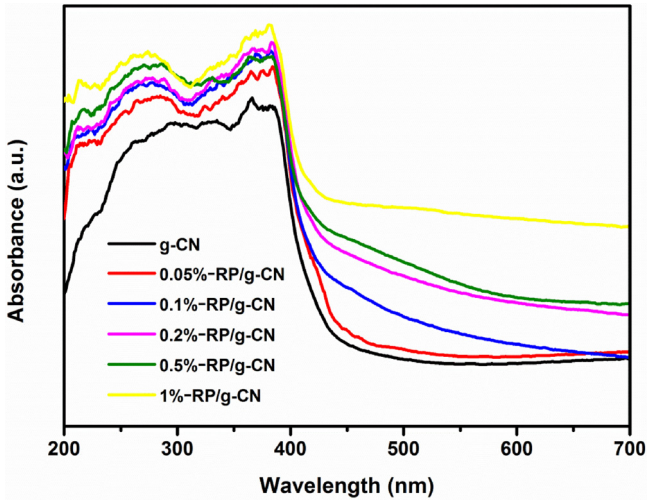

Fig. 4. Diffuse reflectance UV–vis spectra (DRS) of g-CN and RP/g-CN with different ruthenium phosphide contents.

ruthenium phosphide nanoparticles, which were uniformly anchored on the surface of g-CN.

Fig. 3 showed the X-ray diffraction (XRD) patterns of pure g-CN and RP/g-CN composites with different loading amount of ruthenium phosphide. The typical diffraction peaks of pristine g-CN and RP/g-CN samples at 2θ values of 13.1° and 27.4° were assigned to (100) and (002) crystal planes of g-C_3N_4, respectively (JCPDS Card No. 87-1526) [24,32]. The peak at 13.1° corresponded to the in-plane repeating of tris-triazine while d spacing was 0.675 nm. The stronger (002) plane at 27.4° could be indexed to the interplanar structural packing with conjugated aromatic systems along c-axis with the distance of d = 0.326 nm [54,55]. Similar XRD pattern could be seen for RP/g-CN samples as pristine g-CN. No noticeable change could be detected with the RuP concentration from 0.05% to 1%, further suggesting that ruthenium phosphide covered on surface of g-CN nanosheet are with amorphous structures [56].

The photoabsorption performance of g-CN and RP/g-CN composites were analyzed by UV–vis measurements (Fig. 4). As shown in UV–vis diffuse reflectance spectra (DRS), the steep adsorption edge of pristine g-CN and RP/g-CN was ca. 450 nm, corresponding to a 2.75 eV band gap, implying that there was hardly obvious structural change of g-CN after the loading of amorphous ruthenium phosphide [57]. Compared to pure g-CN, the RP/g-CN hybrid exhibited an absorbance intensity increase over the whole range of wavelength, for which the as-prepared RP/g-CN were expected to show better photocatalytic activity. Moreover, the composites displayed enhanced intensive adsorption with the increasing content of RuP which was derived from the intrinsic absorption of black-colored RP/g-CN composites.

The high-resolution XPS spactra were analyzed in order to ascertain the chemical state of C, N, P and Ru. In Fig. 5a, the C 1 s XPS spectra had three distinct peaks at 284.8 eV, 286.4 eV and 288.2 eV, relating to the C—C, C-NH_2, and N—C=N binding, respectively [58]. According to Fig. 5b, the N 1 s peaks located at 398.8 eV, 400 eV and 401 eV, respectively. The peak at 398.8 eV was ascribed to sp^2-hybridized aromatic triazine rings (C—N=C), while the other two peaks at 400 eV and 401 eV were due to the tertiary nitrogen (N-$(C)_3$) and C—NH bonding [60]. As shown in Fig. 5c, three peaks observed at 129.6 eV, 130.4 eV and 133.2 eV. The two peaks at 129.6 eV and 130.4 eV could be assigned to P $2p_{3/2}$ and P $2p_{1/2}$(P^{2-}) in RuP_2, while the peak at 133.2 eV corresponded to P—O species [61,62]. Fig. 5d displayed the high resolution XPS spectrum of Ru 3d. The peaks at 279.5 eV and 280.2 eV could be attributed to Ru° and Ru $3d_{5/2}$ of Ru^{4+} in RuP_2, respectively [50,59,63,64]. The above results further confirmed that the as-obtained sample was composed of g-C_3N_4 and amorphous ruthenium phosphide.

3.2. Hydrogen evolution activity and stability

The photocatalytic HER performance of the samples was tested using triethanolamine (TEOA) as the sacrificial agent under visible light illumination (λ > 420 nm). As illustrated in Fig. 6, pure g-CN showed extremely poor H_2 production of 18.6 μmol h^{-1} g^{-1}. It was also noteworthy that P/g-CN (g-C_3N_4 after phosphatization treatment) also exhibited relatively low H_2 evolution rate (20.9 μmol h^{-1} g^{-1}) due to the rapid recombination of the photogenerated electrons and holes. These results confirmed that the phosphidation treatment alone had a negligible role. It was evident that the H_2 production rate of as-prepared RP/g-CN composites was improved significantly from 0.05%-RP/g-CN to 0.1%-RP/g-CN, then decreased with the increasing weight percent of ruthenium. The 0.1%-RP/g-CN achieved the optimum H_2 evolution rate of 2110 μmol h^{-1} g^{-1}, which was 113.4 times higher than that of pristine g-CN. The weakened photocatalytic performance for 0.2%, 0.5%, 1%-RP/g-CN could be explained by that the overloaded ruthenium phosphide nanoparticles covered on the surface of g-CN resulted in the reduced light energy adsorption of g-CN photosensitizer [65]. In addition, excess RuP nanoparticles would also aggregate together and reduce the active sites on the surface. Moreover, we also investigated the photocatalytic hydrogen production performance of Ru-g-CN. The H_2 evolution rate over Ru-g-CN (287.3 μmol h^{-1} g^{-1}) was much inferior when compared with that of 0.1%-RP/g-CN. Besides, the Pt-loaded g-C_3N_4 photocatalyst (Pt-g-CN) was prepared by an in-situ photodeposition approach and exhibited a lower hydrogen production rate of 952 μmol h^{-1} g^{-1}. The above results indicated that the addition of ruthenium phosphide fully played the role of a cocatalyst for g-CN. The obtained RP/g-CN hybrid showed a much higher H_2 evolution activity than Pt-g-CN, Which could be attributed to the introduce of evenly dispersed amorphous ruthenium phosphide and the interaction of g-CN and ruthenium phosphide cocatalyst. It was worth to point out that the hydrogen evolution rate of 0.1%-RP/g-CN was higher than other g-CN based materials as shown in supporting information (Table S1).

Fig. 7 showed the recycle ability of 0.1%-RP/g-CN in 20 h under the same condition. There was no significant decrease of hydrogen production amount after 5 cycles. The photocatalytic performance remained quite stable after 20 h, revealing an excellent reusability of g-CN decorated by amorphous ruthenium phosphide cocatalyst. The TEM and XPS spectra of the recycled 0.1%-RP/g-CN photocatalysts were also analyzed (Fig. S1-2). It should be mentioned that some positive Ru in ruthenium phosphide are reduced to Ru° after the HER. However,

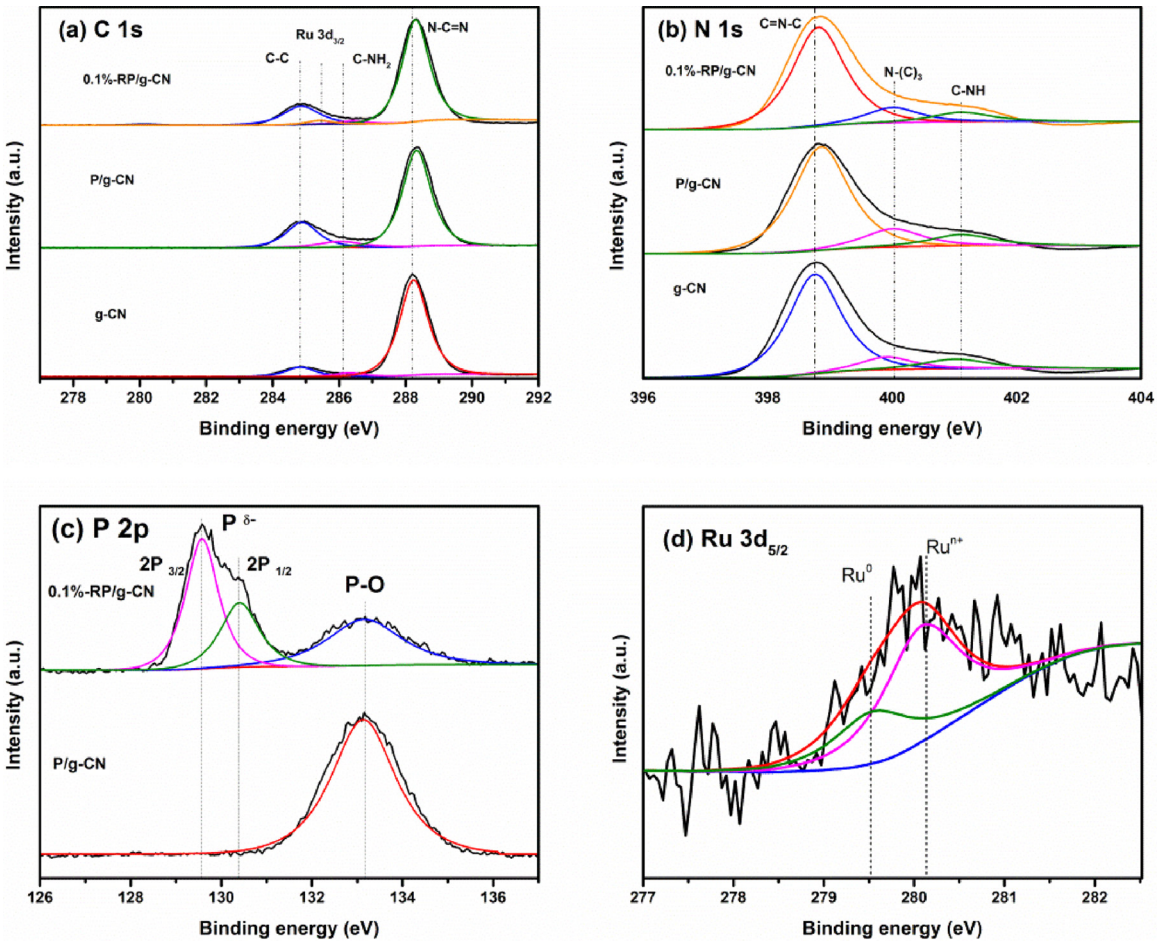

Fig. 5. The XPS spectra of g-CN, P/g-CN and 0.1%-RP/g-CN. (a) C 1 s, (b) N 1 s, (c) P 2p, (d) Ru 3d.

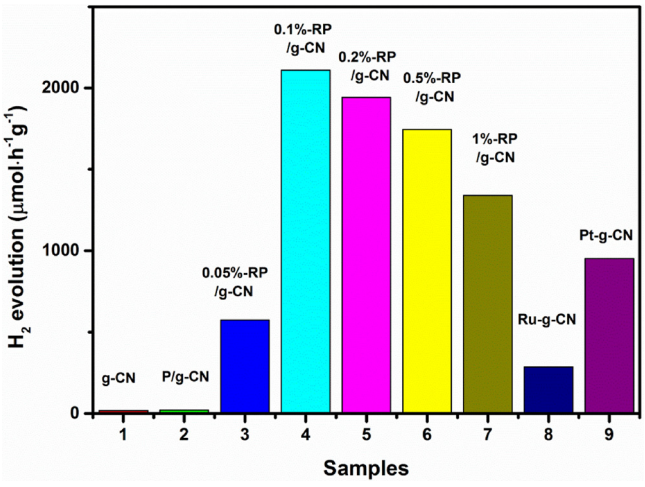

Fig. 6. Comparison of the average hydrogen evolution rate of pure g-CN, P/g-CN, RP/g-CN composites, Ru-g-CN and Pt-g-CN.

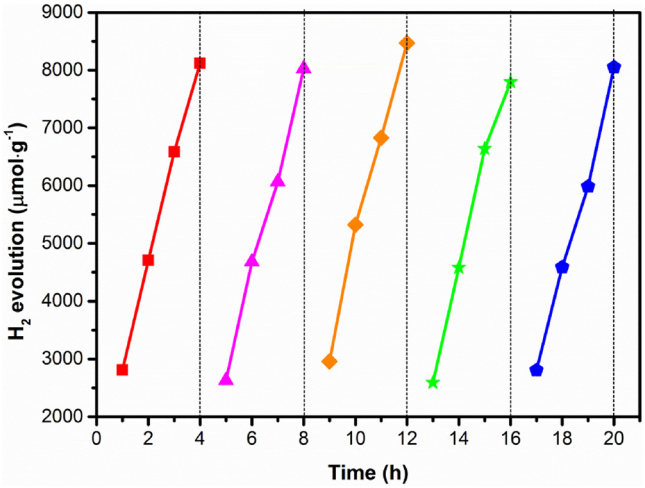

Fig. 7. Cycling test of 0.1%-RP/g-CN for the H_2 generation ability.

according to the previous works [66,67], Ru nanoparticles were also excellent cocatalyst for hydrogen evolution reaction. Therefore, the hydrogen evolution performance was not affected during the recycling experiments.

3.3. Proposed mechanism for the enhanced activity

The transient photocurrent response of pure g-CN and 0.1%-RP/g-CN under visible light was measured in 0.5 M Na_2SO_4 solution with the potential of 0.3 V vs Ag/AgCl electrode. As shown in Fig. 8, it was clear that the photocurrent of 0.1%-RP/g-CN was significantly improved as compared to that of pure g-CN. The photocurrent intensity of 0.1%-RP/g-CN was almost 3 times higher than that of bare g-CN, implying a faster charge transfer efficiency. Furthermore, the electrochemical impedance spectroscopy (Fig. 9) was employed to characterize the electron separation efficiency. The smaller radius for 0.1%-RP/g-CN proved the facilitated interfacial charge transfer between g-CN and amorphous

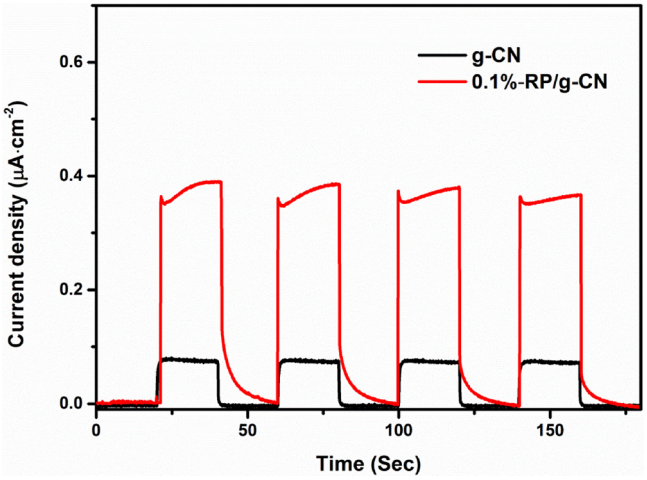

Fig. 8. Transient photocurrent response of pure g-CN and 0.1%-RP/g-CN at bias 0.3 V (vs. SCE).

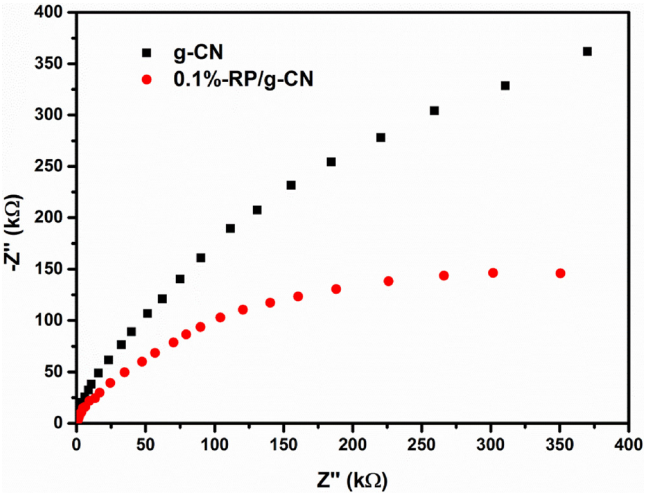

Fig. 9. Electrochemical impedance spectroscopy (EIS) Nyquist plots of g-CN and 0.1%-RP/g-CN composite.

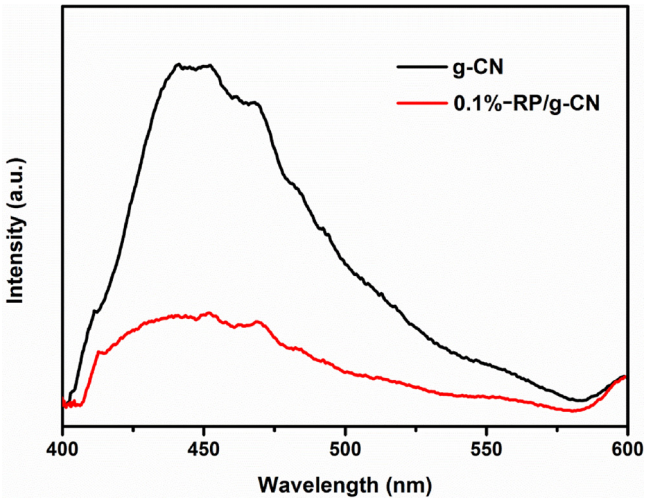

Fig. 10. The photoluminescence spectra of g-CN and 0.1%-RP/g-CN composite.

ruthenium phosphide cocatalyst.

The overpotential for electrochemical H_2 evolution over pure g-CN and 0.1-RP/g-CN was also investigated by the LSV method. As shown in

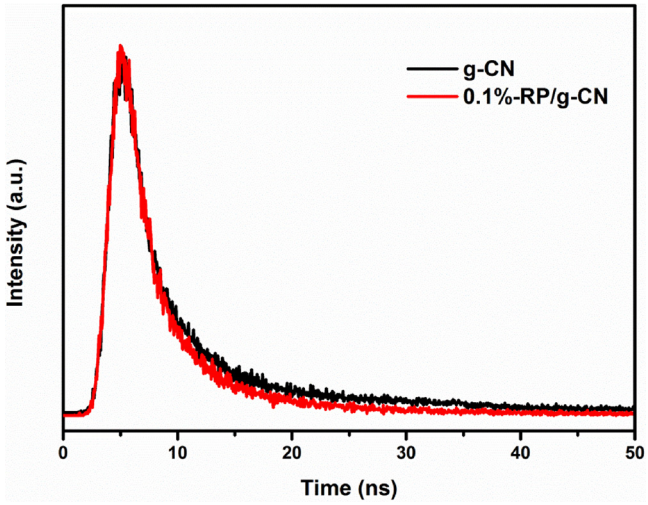

Fig. 11. Time-resolved PL decay plots of g-CN and 0.1%-RP/g-CN composite.

supporting information (Fig. S3), 0.1%-RP/g-CN exhibited much lower overpotential for hydrogen evolution compared with g-CN, implying that ruthenium phosphide quantum dots could acted as efficient cocatalyst to accelerate the sluggish H_2 evolution kinetics over g-CN [68,69].

For further understanding the trapping, migration and recombination process of 0.1%-RP/g-CN, the PL emission spectra (Fig. 10) of pure g-CN and 0.1 wt% RP/g-CN with the excitation wavelength of 200 nm was carried out to measure the recombination rate of charge carriers. For g-C_3N_4, a strong emission peak at about 450 nm could be seen, owning to the ultrafast recombination of excited electron-hole pairs. However, the intensity of 0.1%-RP/g-CN was considerably reduced, suggesting that the electrons generated by g-CN migrated to the well dispersed amorphous ruthenium phosphide nanoparticles and thus restrained the recombination of charge carriers. To prove the more effective interfacial charge transfer of the prepared samples, the time-resolved photoluminescences (TRPL) of g-CN and 0.1%-RP/g-CN were measured and the obtained results are shown in Fig. 11. The emission lifetime of pristine g-CN was 7.44 ns, whereas 0.1%-RP/g-CN exhibited a lifetime of 5.56 ns. The significantly decreased lifetime of 0.1%-RP/g-CN can be attributed to rapid interfacial electron transfer from g-CN to amorphous ruthenium phosphide nanoparticles, suggesting that more electrons would participate in hydrogen evolution process [23,70].

Considering all of the information above, the possible photocatalytic mechanism over g-CN modified by ultrafine amorphous ruthenium phosphide nanoparticles uniformly was speculated as shown in Fig. 12. Upon visible light excitation, electron-hole pairs were generated in g-CN. Unfortunately, the inherently fast recombination of photo-generated charge carriers of pristine g-CN greatly restricted its activity. However, the addition of well dispersed ultrafine amorphous ruthenium phosphide nanoparticles leaded to the formation of a large number of active sites on the surface of g-CN. The amorphous ruthenium phosphide cocatalysts could provided an outlet for the electrons generated from g-CN. On the one hand, the recombination of electron-hole pairs were dramatically suppressed because of the factor that electrons quickly transferred to well dispersed amorphous ruthenium phosphide and holes were consumed by the sacrificial agent of TEOA. On the other hand, the presence of ultrafine amorphous ruthenium phosphide allowed the electrons to rapidly combine with protons to generate hydrogen. Meanwhile, loading ruthenium phosphide quantum dots could also accelerate the hydrogen evolution kinetics which was caused by the decreased overpotential. In this way, the electron transfer rate was enhanced and the recombination was restricted, which could significantly improve the photocatalytic hydrogen evolution performance.

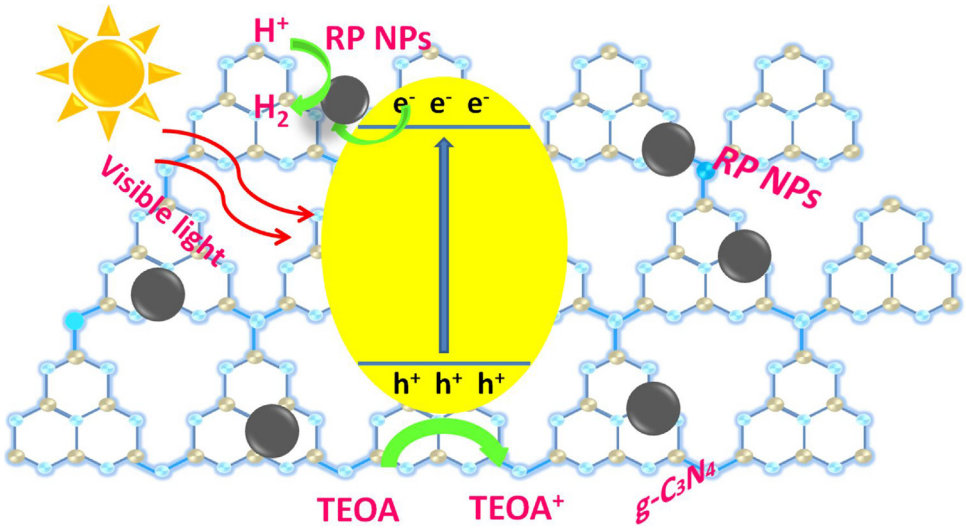

Fig. 12. The proposed photocatalytic mechanism of 0.1%-RP/g-CN for H_2 evolution.

4. Conclusions

To sum up, we have demonstrated that g-CN modified by ultrafine amorphous ruthenium phosphide nanoparticles is a very robust photocatalyst for hydrogen evolution reaction. The optimum H_2 generation rate for 0.1%-RP/g-CN reached up to 2110 $\mu mol\, h^{-1}\, g^{-1}$, which was 2.2 times higher than that of Pt-g-CN, hence enabled it a cheaper alternative to Pt-based photocatalysts. The optimum 0.1%-RP/g-CN with a low content of Ru provided it a huge economical advantage in price over Pt-g-CN. The ultrafine ruthenium phosphide nanoparticles uniformly supported on the surface and the interaction between ruthenium phosphide cocatalyst and g-CN contributed together to the faster transfer of photoexcited electrons and less recombination of electron-hole pairs. The results offer a new avenue to develop outstanding hydrogen evolution photocatalysts while reducing the cost of noble metal.

Acknowledgements

We are grateful for grants from National Science Funds for Creative Research Groups of China (No. 51421006), Natural Science Foundation of China (51679063), the Fundamental Research Funds for The Central Universities (2018B14514), the Key Program of National Natural Science Foundation of China (No. 91647206), the National Key Plan for Research and Development of China (2016YFC0502203), and PAPD.

Appendix A. Supplementary data

Supplementary material related to this article can be found, in the online version, at doi:https://doi.org/10.1016/j.apcatb.2018.08.048.

References

[1] Z.P. Yan, Z.J. Sun, X. Liu, H.X. Jia, P.W. Du, Cadmium sulfide/graphitic carbon nitride heterostructure nanowire loading with a nickel hydroxide cocatalyst for highly efficient photocatalytic hydrogen production in water under visible light, Nanoscale 8 (2016) 4748–4756.

[2] A. Indra, A. Acharjya, P.W. Menezes, C. Merschjann, D. Hollmann, M. Schwarze, M. Aktas, A. Friedrich, S. Lochbrunner, A. Thomas, M. Driess, Boosting visible-light-driven photocatalytic hydrogen evolution with an integrated nickel phosphide-carbon nitride system, Angew. Chem. Int. Ed. 56 (2017) 1653–1657.

[3] G.S. Li, Z.C. Lian, W.C. Wang, D.Q. Zhang, H.X. Li, Nanotube-confinement induced size-controllable g-C_3N_4 quantum dots modified single-crystalline TiO_2 nanotube arrays for stable synergetic photoelectrocatalysis, Nano Energy 19 (2016) 446–454.

[4] G. Zhou, M.F. Wu, Q.J. Xing, F. Li, H. Liu, X.B. Luo, J.P. Zou, J.M. Luo, A.Q. Zhang, Synthesis and characterizations of metal-free semiconductor/MOFs with good stability and high photocatalytic activity for H_2 evolution: a novel Z-scheme heterostructured photocatalyst formed by covalent bonds, Appl. Catal. B: Environ. 220 (2018) 607–614.

[5] Z.C. Lian, W.C. Wang, G.S. Li, F.H. Tian, K.S. Schanze, H.X. Li, Pt-enhanced mesoporous Ti^{3+}/TiO_2 with rapid bulk to surface Electron transfer for photocatalytic hydrogen evolution, ACS Appl. Mater. Interfaces 9 (2017) 16959–16966.

[6] X.J. Fan, H.Q. Zhou, X. Guo, WC nanocrystals grown on vertically aligned carbon nanotubes: an efficient and stable electrocatalyst for hydrogen evolution reaction, ACS Nano 9 (2015) 5125–5134.

[7] T. Wang, X.J. Wang, Y. Liu, J. Zheng, X.G. Li, A highly efficient and stable biphasic nanocrystalline Ni–Mo–N catalyst for hydrogen evolution in both acidic and alkaline electrolytes, Nano Energy 22 (2016) 111–119.

[8] Y.M. Shi, B. Zhang, Recent advances in transition metal phosphide nanomaterials: synthesis and applications in hydrogen evolution reaction, Chem. Soc. Rev. 45 (2016) 1781-1781.

[9] J.W. Su, Y. Yang, G.L. Xia, J.T. Chen, J. Peng, Q.W. Chen, Ruthenium-cobalt nanoalloys encapsulated in nitrogen-doped graphene as active electrocatalysts for producing hydrogen in alkaline media, Nat. Commun. 8 (2017) 14969.

[10] Q. Guo, C.Y. Zhou, Z.B. Ma, Z.F. Ren, H.J. Fan, X.M. Yang, Elementary photocatalytic chemistry on TiO_2 surfaces, Chem. Soc. Rev. 45 (2016) 3701–3730.

[11] C.P. Sajan, S. Wageh, A.A. Al-Ghamdi, J.G. Yu, S.W. Cao, TiO_2 nanosheets with exposed {001} facets for photocatalytic applications, Nano Res. 9 (2016) 3–27.

[12] X.J. Wang, W.Y. Yang, F.T. Li, Y.B. Xue, R.H. Liu, Y.J. Hao, In situ microwave-assisted synthesis of porous N-TiO_2/g-C_3N_4 heterojunctions with enhanced visible-light photocatalytic properties, Ind. Eng. Chem. Res. 52 (2013) 17140–17150.

[13] L.M. Song, T.T. Li, S.J. Zhang, S.N. Zhang, Synthesis of rhodium phosphide cocatalyst and remarkably enhanced photocatalytic hydrogen evolution over CdS under visible light radiation, Chem. Eng. J. 314 (2017) 498–507.

[14] N.N. Chai, H.X. Wang, C.X. Hu, Q. Wang, H.L. Zhang, Well-controlled layer-by-layer assembly of carbon dots/CdS heterojunction for efficient visible-light-driven photocatalysis, J. Mater. Chem. A 3 (2015) 16613–16620.

[15] B. Han, S. Liu, N. Zhang, Y.J. Xu, Z.R. Tang, One-dimensional CdS@MoS_2 core-shell nanowires for boosted photocatalytic hydrogen evolution under visible light, Appl. Catal. B: Environ. 202 (2017) 298–304.

[16] Y.M. Zhong, J.L. Yuan, J.Q. Wen, X. Li, Y.H. Xu, W. Liu, S.S. Zhang, Y.P. Fang, Earth-abundant NiS co-catalyst modified metal-free mpg-C_3N_4/CNT nanocomposites for highly efficient visible-light photocatalytic H_2 evolution, Dalton Trans. 44 (2015) 18260–18269.

[17] G.C. Bi, J.Q. Wen, X. Li, W. Liu, J. Xie, Y.P. Fang, W.W. Zhang, Efficient visible-light photocatalytic H_2 evolution over metal-free g-C_3N_4 co-modified with robust acetylene black and $Ni(OH)_2$ as dual co-catalysts, RSC Adv. 6 (2016) 31497–31506.

[18] J.Q. Wen, J. Xie, X.B. Chen, X. Li, A review on g-C_3N_4-based photocatalysts, Appl. Surf. Sci. 391 (2016) 72–123.

[19] X. Li, X.F. Zhou, Q.Z. Gao, J.L. Yuan, J.Q. Wen, Y.P. Fang, W. Liu, S.S. Zhang, Y.J. Liu, Metal-free carbon nanotube–SiC nanowire heterostructures with enhanced photocatalytic H_2 evolution under visible light irradiation, Catal. Sci. Technol. 5 (2015) 2798–2806.

[20] L.X. Chen, F. He, C.S. Shi, C.N. He, E.Z. Liu, L.Y. Ma, N.Q. Zhao, Fabrication of Er/Tm/Yb/Y_2O_3 upconversion luminescence enhanced 3C-SiC composites as highly UV–Vis–NIR light responsive photocatalysts, J. Alloys 740 (2018) 719–726.

[21] H.L. Wang, L.S. Zhang, Z.G. Chen, J.Q. Hu, S.J. Li, Z.H. Wang, J.S. Liu, X.C. Wang, Semiconductor heterojunction photocatalysts: design, construction, and photocatalytic performances, Chem. Soc. Rev. 43 (2014) 5234–5244.

[22] L. Ma, X.X. Kang, S.Z. Hu, F. Wang, Preparation of Fe, P, Co-doped graphitic carbon nitride with enhanced visible-light photocatalytic activity, J. Mol. Catal. 29 (2015) 359–368.

[23] D.Q. Zeng, W.J. Xu, W.J. Ong, J. Xu, H. Ren, Y.Z. Chen, H.F. Zheng, D.L. Peng, Toward noble-metal-free visible-light-driven photocatalytic hydrogen evolution: monodisperse sub–15 nm Ni_2P nanoparticles anchored on porous g-C_3N_4 nanosheets to engineer 0D-2D heterojunction interfaces, Appl. Catal. B: Environ. 221 (2017) 47–55.

[24] S.S. Yi, J.M. Yan, B.R. Wulan, S.J. Li, K.H. Liu, Q. Jiang, Noble-metal-free cobalt phosphide modified carbon nitride: an efficient photocatalyst for hydrogen generation, Appl. Catal. B: Environ. 200 (2017) 477–483.

[25] J. Wang, Z. Yang, X.X. Gao, W.Q. Yao, W.Q. Wei, X.J. Chen, R.L. Zong, Y.F. Zhu, Core-shell g-C_3N_4@ZnO composites as photoanodes with double synergistic effects for enhanced visible-light photoelectrocatalytic activities, Appl. Catal. B: Environ. 217 (2017) 169–180.

[26] X.H. Wu, F.Y. Chen, X.F. Wang, H.G. Yu, In situ one-step hydrothermal synthesis of oxygen-containing groups-modified g-C_3N_4 for the improved photocatalytic H_2-evolution performance, Appl. Surf. Sci. 427 (2018) 645–653.

[27] X.Q. Hao, J. Zhou, Z.W. Cui, Y.C. Wang, Y. Wang, Z.G. Zou, Zn-vacancy mediated electron-hole separation in ZnS/g-C_3N_4 heterojunction for efficient visible-light photocatalytic hydrogen production, Appl. Catal. B: Environ. 229 (2018) 41–51.

[28] J.P. Zou, L.C. Wang, J. Luo, Y.C. Nie, Q.J. Xing, X.B. Luo, H.M. Du, S.L. Luo, S.L. Suib, Synthesis and efficient visible light photocatalytic H_2 evolution of a metal-free g-C_3N_4/graphene quantum dots hybrid photocatalyst, Appl. Catal. B: Environ. 193 (2016) 103–109.

[29] G.M. Jiang, X.W. Li, M.N. Lan, T. Shen, X.S. Lv, F. Dong, S. Zhang, Monodisperse bismuth nanoparticles decorated graphitic carbon nitride: enhanced visible-light-response photocatalytic NO removal and reaction pathway, Appl. Catal. B: Environ. 205 (2017) 532–540.

[30] M. Zhang, J. Xu, R.L. Zong, Y.F. Zhu, Enhancement of visible light photocatalytic activities via porous structure of g-C_3N_4, Appl. Catal. B: Environ. 147 (2014) 229–235.

[31] F. Dong, Z. Zhao, Y. Sun, Y. Zhang, S. Yan, Z. Wu, An advanced semimetal–organic Bi spheres–g-C_3N_4 nanohybrid with SPR-enhanced visible-light photocatalytic performance for NO purification, Environ. Sci. Technol. 49 (2015) 12432–12440.

[32] G. Liu, P. Niu, C.H. Sun, S.C. Smith, Z.G. Chen, G.Q. Lu, H.M. Cheng, Unique electronic structure induced high photoreactivity of sulfur-doped graphitic C_3N_4, J. Am. Chem. Soc. 132 (2010) 11642–11648.

[33] Y.J. Wang, Z.X. Wang, S. Muhammad, J. He, Graphite-like C_3N_4 hybridized $ZnWO_4$ nanorods: synthesis and its enhanced photocatalysis in visible light, CrystEngComm 14 (2012) 5065–5070.

[34] D.Q. Zeng, W.J. Ong, H.F. Zheng, M.D. Wu, Y.Z. Chen, D.L. Peng, M.Y. Han, $Ni_{12}P5$ nanoparticles embedded into porous g-C_3N_4 nanosheets as a noble-metal-free hetero-structure photocatalyst for efficient H_2 production under visible light, J. Mater. Chem. A 5 (2017) 16171–16178.

[35] H.G. Yu, P.A. Xiao, P. Wang, J.G. Yu, Amorphous molybdenum sulfide as highly efficient electron-cocatalyst for enhanced photocatalytic H_2 evolution, Appl. Catal. B Environ. 193 (2016) 217–225.

[36] Y.B. Chen, Z.X. Qin, General applicability of nanocrystalline Ni_2P as a noble-metal-free cocatalyst to boost photocatalytic hydrogen generation, Catal. Sci. Technol. 6 (2016) 8212–8221.

[37] W.J. Wang, T.C. An, G.Y. Li, D.H. Xia, H.J. Zhao, J.C. Yu, P.K. Wong, Earth-abundant Ni_2P/g-C_3N_4 lamellar nanohydrids for enhanced photocatalytic hydrogen evolution and bacterial inactivation under visible light irradiation, Appl. Catal. B: Environ. 217 (2017) 570–580.

[38] D.S. Dai, H. Xu, L. Ge, C.C. Han, Y.Q. Gao, S.S. Li, Y. Lu, In-situ synthesis of CoP co-catalyst decorated $Zn_{0.5}Cd_{0.5}S$ photocatalysts with enhanced photocatalytic hydrogen production activity under visible light irradiation, Appl. Catal. B: Environ. 217 (2017) 429–436.

[39] D. Zhao, B. Sun, X.Q. Li, L.X. Qin, S.Z. Kang, D. Wang, Promoting visible light-driven hydrogen evolution over CdS nanorods using earth-abundant CoP as a co-catalyst, RSC Adv. 6 (2016) 33120–33125.

[40] Q.D. Yue, Y.Y. Wan, Z.J. Sun, X.J. Wu, Y.P. Yuan, P.W. Du, MoP is a novel, noble-metal-free cocatalyst for enhanced photocatalytic hydrogen production in water under visible light, J. Mater. Chem. A 3 (2015) 16941–16947.

[41] S. Rundqvist, A. Hede, E. Varde, G. Westin, The structures of Co_2P, Ru_2P, and related phases, Acta Chem. Scand. 14 (1960) 1961–1979.

[42] H. Zhao, S.N. Sun, P.P. Jiang, Z.J. Xu, Graphitic C_3N_4 modified by Ni_2P cocatalyst: an efficient, robust and low cost photocatalyst for visible-light-driven H_2 evolution from water, Chem. Eng. J. 315 (2017) 296–303.

[43] M.M. Rashid, M.K.A. Mesfer, H. Naseem, M. Danish, Hydrogen production by water electrolysis: a review of alkaline water electrolysis, PEM water electrolysis and high temperature water electrolysis, Inter. J. Eng. Adv. Tech. 4 (2015) 2249–8958.

[44] L.L. Zhu, H.P. Lin, Y.Y. Li, F. Liao, Y. Lifshitz, M.Q. Sheng, S.T. Lee, M.W. Shao, A rhodium/silicon co-electrocatalyst design concept to surpass platinum hydrogen evolution activity at high overpotentials, Nat. Commun. 7 (2016) 12272.

[45] T. Bhowmik, M.K. Kundu, S. Barman, Palladium nanoparticle–graphitic carbon nitride porous synergistic catalyst for hydrogen evolution/oxidation reactions over a broad range of pH and correlation of its catalytic activity with measured hydrogen binding energy, ACS Catal. 6 (2016) 1929–1941.

[46] C.S. Lim, Z. Sofer, R.J. Toh, A.Y.S. Eng, J. Luxa, M. Pumera, Iridium-and osmium-decorated reduced graphenes as promising catalysts for hydrogen evolution, ChemPhysChem 16 (2015) 1898–1905.

[47] X.K. Kong, K. Xu, C.L. Zhang, J. Dai, S.N. Oliaee, L.Y. Li, X.C. Zeng, C.Z. Wu, Z.M. Peng, Free-standing two-dimensional Ru nanosheets with high activity toward water splitting, ACS Catal. 6 (2016) 1487–1492.

[48] Y. Peng, B.Z. Lu, L.M. Chen, N. Wang, J.E. Lu, Y. Ping, S.W. Chen, Hydrogen evolution reaction catalyzed by ruthenium ion-complexed graphitic carbon nitride nanosheets, J. Mater. Chem. A 5 (2017) 18261–18269.

[49] C. Kong, Y.X. Han, L.J. Hou, D.P. Chen, B.W. Wu, Effect of synthetic method and reductant on the morphology and photocatalytic hydrogen evolution performance of Ru nanoparticles, Chem. Res 33 (2017) 1–6 in Chinese U.

[50] T.T. Liu, S. Wang, Q.J. Zhang, L. Chen, W.H. Hu, C.M. Li, Ultrasmall Ru_2P nanoparticles on graphene: a highly efficient hydrogen evolution reaction electrocatalyst in both acidic and alkaline media, Chem. Commun. 54 (2018) 3343–3346.

[51] W. Liu, L.L. Cao, W.R. Cheng, Y.J. Cao, X.K. Liu, W. Zhang, X.L. Mou, L.L. Jin, X.S. Zheng, W. Che, Q.H. Liu, T. Yao, S.Q. Wei, Single-site active cobalt-based photocatalyst with long carriers lifetime for spontaneous overall water splitting, Angew. Chem. Int. Ed. 56 (2017) 9312–9317.

[52] F. Dong, L.W. Wu, Y.J. Sun, M. Fu, Z.B. Wu, S.C. Lee, Efficient synthesis of polymeric g-C_3N_4 layered materials as novel efficient visible light driven photocatalysts, J. Mater. Chem. 21 (2011) 15171–15174.

[53] Z.H. Pu, I.S. Amiinu, Z.H. Kou, W.Q. Li, S.C. Mu, RuP_2-based catalysts with platinum-like activity and higher durability for hydrogen evolution reaction at all pH values, Angew. Chem. Int. Ed. 56 (2017) 11559–11564.

[54] X.C. Wang, K. Maeda, A. Thomas, K. Takanabe, G. Xin, J.M. Carlsson, K. Domen, M. Antonietti, A metal-free polymeric photocatalyst for hydrogen production from water under visible light, Nat. Mater. 8 (2009) 76–80.

[55] J.H. Sun, J.S. Zhang, M.W. Zhang, M. Antonietti, X.Z. Fu, X.C. Wang, Bioinspired hollow semiconductor nanospheres as photosynthetic nanoparticles, Nat. Commun. 3 (2012) 1139.

[56] M.G. Li, M.P. Yu, X. Li, Improving the catalytic activity of amorphous molybdenum sulfide for hydrogen evolution reaction using polydihydroxyphenylalanine modified MWCNTs, Appl. Surf. Sci. 439 (2018) 343–349.

[57] H. Zhao, J.W. Wang, Y.M. Dong, P.P. Jiang, Noble-metal-free iron phosphide co-catalyst loaded graphitic carbon nitride as an efficient and robust photocatalyst for hydrogen evolution under visible light irradiation, ACS Sustain. Chem. Eng. 5 (2017) 8053–8060.

[58] X.Z. Yue, S.S. Yi, R.W. Wang, Z.T. Zhang, S.L. Qiu, Cadmium sulfide and nickel synergetic co-catalysts supported on graphitic carbon nitride for visible-light-driven photocatalytic hydrogen evolution, Sci. Rep. 6 (2016) 22268.

[59] Q.B. Chang, J.W. Ma, Y.Z. Zhu, Z. Li, D.Y. Xu, X.Z. Duan, W.C. Peng, Y. Li, G.L. Zhang, F.B. Zhang, Controllable synthesis of ruthenium phosphides (RuP and RuP_2) for pH-Universal hydrogen evolution reaction, ACS Sus. Chem. Eng. 6 (2018) 6388–6394.

[60] S.L. Ma, S.H. Zhan, Y.N. Jia, Q. Shi, Q.X. Zhou, Enhanced disinfection application of Ag-modified g-C_3N_4 composite under visible light, Appl. Catal. B: Environ. 186 (2016) 77–87.

[61] S.Z. Hu, L. Ma, J.G. You, F.Y. Li, Z.P. Fan, G. Lu, D. Liu, J.Z. Gui, Enhanced visible light photocatalytic performance of g-C_3N_4 photocatalysts co-doped with iron and phosphorus, Appl. Surf. Sci. 311 (2014) 164–171.

[62] X.G. Ma, Y.H. Lv, J. Xu, Y.F. Liu, R.Q. Zhang, Y.F. Zhu, A strategy of enhancing the photoactivity of g-C_3N_4 via doping of nonmetal elements: a first-principles study, J. Phys. Chem. C 116 (2012) 23485–23493.

[63] D.J. Morgan, Resolving ruthenium: XPS studies of common ruthenium materials, Surf. Interface Anal. 47 (2015) 1072–1079.

[64] K. Brousse, S. Nguyen, A. Gillet, S. Pinaud, R. Tan, A. Meffre, K. Soulantica, B. Chaudret, P.L. Taberna, M. Respaud, P. Simon, Laser-scribed Ru organometallic complex for the preparation of RuO_2 micro-supercapacitor electrodes on flexible substrate, Electrochim. Acta 281 (2018) 816–821.

[65] Z.J. Sun, B.H. Lv, J.S. Li, M. Xiao, X.Y. Wang, P.W. Du, Core-shell amorphous cobalt phosphide/cadmium sulfide semiconductor nanorods for exceptional photocatalytic hydrogen production under visible light, J. Mater. Chem. A 4 (2015) 1598–1602.

[66] J. Wang, Z.Z. Wei, S.J. Mao, H.R. Li, Y. Wang, Highly uniform Ru nanoparticles over N-doped carbon: pH and temperature-universal hydrogen release from water reduction, Energy Environ. Sci. 11 (2018) 800–806.

[67] C. Kong, Z. Li, G.X. Lu, The dual functional roles of Ru as co-catalyst and stabilizer of dye for photocatalytic hydrogen evolution, Int. J. Hydrgen Energy 40 (2015) 5824–5830.

[68] W. Zhen, X. Ning, B. Yang, Y. Wu, Z. Li, G. Lu, The enhancement of CdS photocatalytic activity for water splitting via anti-photocorrosion by coating Ni_2P shell and removing nascent formed oxygen with artificial gill, Appl. Catal. B: Environ. 221 (2017) 243–257.

[69] K.L. He, J. Xie, M.L. Li, X. Li, In situ one-pot fabrication of g-C_3N_4 nanosheets/NiS cocatalyst heterojunction with intimate interfaces for efficient visible light photocatalytic H_2 generation, Appl. Surf. Sci. 430 (2018) 208–217.

[70] B.R. Wulan, S.S. Yi, S.J. Li, Y.X. Duan, J.M. Yan, Q. Jiang, Amorphous nickel pyrophosphate modified graphitic carbon nitride: an efficient photocatalyst for hydrogen generation from water splitting, Appl. Catal. B: Environ. 231 (2018) 43–50.